Title: studies of correlated x-ray scattering at Angstrom resolution

Authors: Derek Mendez, Thomas-Joseph Lane, Jongmin Sung, Clèment Levard, Daniel Ratner, Sebastian Doniach

1. The promise: Wochner et al (2009) showed that local order within disorder could be extracted for colloidal gels of polymethylmethacrylate (PMMA) based on an X-ray cross correlation analysis. This followed early work by Kam [ref] showing that measurement of angular correlations of x-ray scattering from an ensemble of randomly oreinted biomolecules could in principle give information about the internal structure of the molecules not attainable from simple x-ray scattering measurements.

Specifically, if the number of photons falling on pixels q_1 and q_2 at scattering vectors $\vec{q_1}, \vec{q_2}$, are denoted by n_{q_1} and n_{q_2} then the correlator

$$C(q_1, q_2, \psi) = \langle n_{q_1} n_{q_2} \rangle - \langle n_{q_1} \rangle \langle n_{q_2} \rangle \tag{1}$$

where ψ is the angle between the scattering vectors $\vec{q_1}$ and $\vec{q_1}$, and $\langle n_q \rangle$ denotes the angular average at constant q, may be written in terms of a Legendre series as

$$C(\vec{q_1}, \vec{q_2}) = \frac{N}{4\pi} \sum_l P_l(\cos(\psi)) C_l(|q_1|, |q_2|) \equiv C(|q_1|, |q_2|, \psi). \tag{2}$$

C_l may be calculated directly from the molecular scattering $|F(\vec{q})|^2$ where F is the form factor of the molecule

$$F(\vec{q}) = \sum_i f_i e^{i\vec{q} \cdot \vec{r}_i} \tag{3}$$

and $\vec{r}_i$ are the atomic coordinates.

Thus, in principle measurement of Correlated X-ray Scattering (CXS) at large angles giving scattering vectors on the same scale as those used in macromolecular crystallography, allows experimentally measurable bounds to be placed on the values of $|F(\vec{q})|^2$. Hence it may be expected that CXS can be used to refine an atomic resolution model of the macromolecule, thus improving our knowledge of the molecular structure in cases where suitable crystals are not attainable. Furthermore, using an xFEL will allow for snapshot measurements at atomic resolution, in tens of femtoseconds, of changes in conformation of a molecule.

2. the challenge. The correlations in equn(2) arise from events where pairs of scatterings into pixels q_1, q_2 arise from the *same* molecule. However, as shown by Kirian et al [ref] there is an intrinsic background in the CXS measurement resulting from pairs of scattering events into the *same* pairs of pixels q_1, q_2 but arising from independent scatterings from *different* molecules. Furthermore, Kirian et al showed that the numbers of uncorrelated double scattering events (UDS) scales with the number of molecules in the x-ray shot in the same way as occurs for the the correlated double scattering events (CDS). This gives rise to a challenge: how to separate the contributions of the CDS events from the that for the UDS events in the measured correlators?

3. **A solution for the case of metallic nanoparticles.** To tackle this problem, we investigated CXS from a series of samples of 20nm silver nanoparticles (NPs) embedded in a glycerol solution and maintained at 100°K in a cryo stream to avoid rotational Brownian motion during 0.5 to 0.7 sec exposures in the micro-focus x-ray beam set at 17 keV (beam line 12-2) at SSRL. (see details in experimental section below.) Around 11,000 screen shots were recorded using a Pilatus 6M detector. In each shot around 10^8 NPs contributed to the observed scattering. Initial attempts to see convergence of the auto correlators computed at the strongest "Bragg ring" by taking the mean over thousands of shots (after removing outliers as discussed in section 6) were unsuccessful. The intrinsic background noise was comparable in strength to the CDS contributions.

However when we converted the observed scattering intensities $s(\varphi)$ at azimuthal angles φ to a binary scale in which values of s below the standard deviation over a series of shots were set to zero and all values of $s(\varphi)$ greater than this threshold value were set equal to unity, the mean of the resulting ensemble of values of the correlators $C(q_{\text{bragg}}, \psi, n_{\text{shot}})$ of the $s(\varphi, n_{\text{shot}})$ over the ensemble of shots showed the double peak feature obtained in simulations of CXS from the NPs using a lattice model of 65,000 unit cells of the *fcc* silver lattice contained in a sphere of diameter 20nm. (see figure 2, which was computed for 2nm NPs as opposed to the data which was measured on 20nm NPs.)
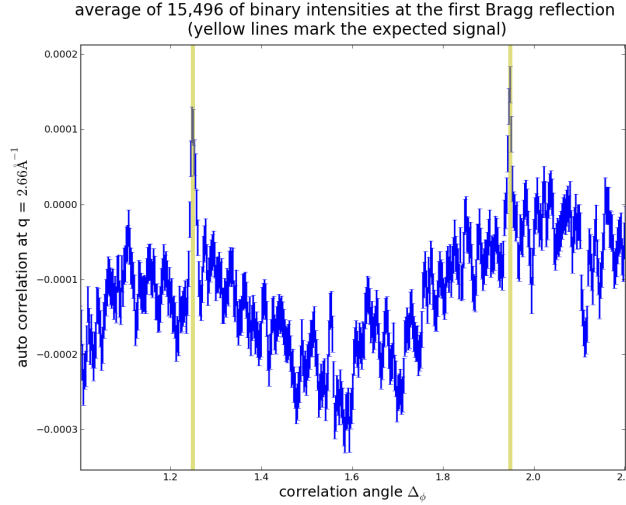

average of 15,496 of binary intensities at the first Bragg reflection
(yellow lines mark the expected signal)

Figure 1: Mean of autocorrelators of15,496 shots of 20nm silver NP scattering after non-linear conversion to binary intensities

4. **Analysis**. Estimates of the number of photons scattered by each NP per shot were on the scale of 3.5 photons/NP/shot. so the possibility of observing a sizeable fraction of CDS events is sizeable (**need estimate!**). The effectiveness of the highly non-linear binary conversion of the observed intensities on the magnitude of the ratio of the amplitude of CDS events to that of the UDS events may be seen by the following argument.

For CDS events we can write for a given shot

$$C(\psi) = \sum_i \int d\phi P_{ns}(\omega_i) \int d\varphi \ s(\varphi, \omega_i) s(\varphi + \psi, \omega_i) \tag{4}$$

2

where all scatterings are assumed to be on the Bragg ring q_{Bragg}. Here $P_{ns}(\omega_i)$ represents the probability of the particles being oriented at Euler angle ω_i in shot $ns = n_{\text{shot}}$.

For UDS events on the other hand,

$$C(\psi) = \int d\varphi \left\{ \sum_i P_{ns}(\omega_i) \, s(\varphi, \omega_i) \right\} \left\{ \sum_j P_{ns}(\omega_j) s(\varphi + \psi, \omega_j) \right\} \tag{5}$$

Since the numbers of orientations per shot are finite, the averages of $s(\varphi, \omega_i)$ over the ω_i will still vary from shot to shot. However these fluctuating averages would not be correlated within a shot, so will tend to converge when averaged over many shots.

For the case of the silver NPs, the angle dependent intensities $s(\varphi, \omega_i)$ are found in simulations (see following section) to vary exponentially with small changes in ω_i as they behave like broadened out Bragg scattering peaks (see fig.). So the probability of scattering into a given pixel varies exponentially as ω_i varies by a small amount. The non-linear transformation induced by re-setting the scale of the $s(\varphi, \omega_i)$ to binary reduces enourmously the fluctuations in the averages of $s(\varphi, \omega_i)$ so that their distributions averaged over in equn.(5) are much more gaussian than the distributions of the raw scattering data. On the other hand for the CDS calculation, equn(4), the gaussian character of the binary-converted data enables a smooth convergence to the mean correlator for the CDS events.

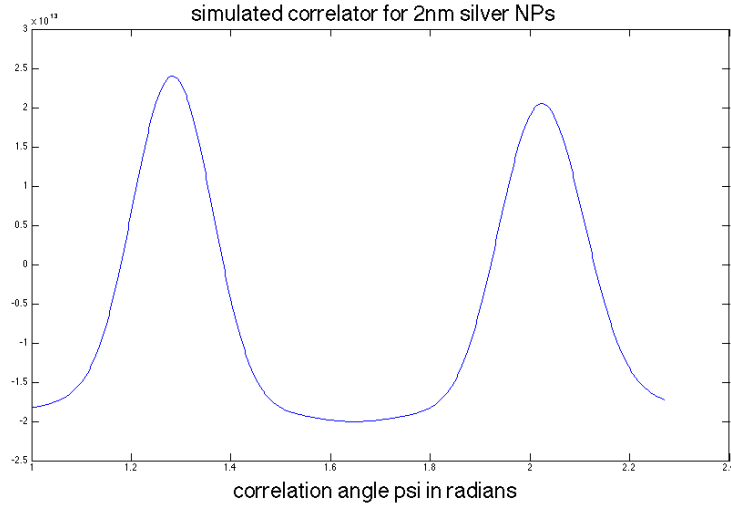5) **simulations** Based on a simple model of the NPs as an fcc lattice of silver atoms placed

Figure 2: simulated correlators for 2nm silver NPs

within a spherical boundary, the expected scattering for one particle will lead to a reciprocal lattice of Bragg reflections broadened by the finite size of the particle. The first Bragg ring for an ensemble of randomly oriented oriented NPs will then be formed by the powder ring of [111] reflections. Within the space of random orientations there will be a subset with satisfy the constraints which produce double Bragg reflections within the first q-ring. It's the latter subset of random orientations which will produce the double scattering events which contribute to the correlator shown in fig 2.

Computation of the correlator $C(q, \psi, \omega_i)$ of the scattering intensity $s(\vec{q}, \omega_i)$ shows exponen-
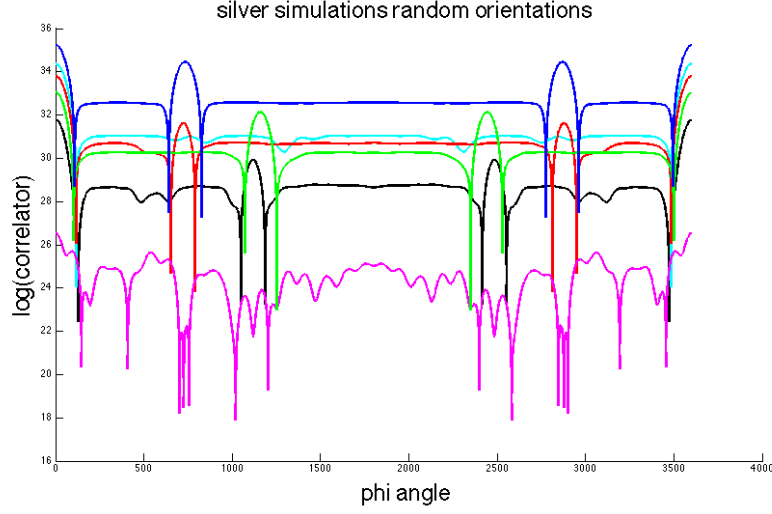
Figure 3: correlators for NP simulation at a variety of random orientations showing exponential variation

tial variation as the orientation ω_i varies, as shown in figs 3,4. It is this large variation which prevents convergence of the UDS component of the signal, making the non-linear treansform to binary signal intensities effective for inducing convergence of the UDS component of the signal.
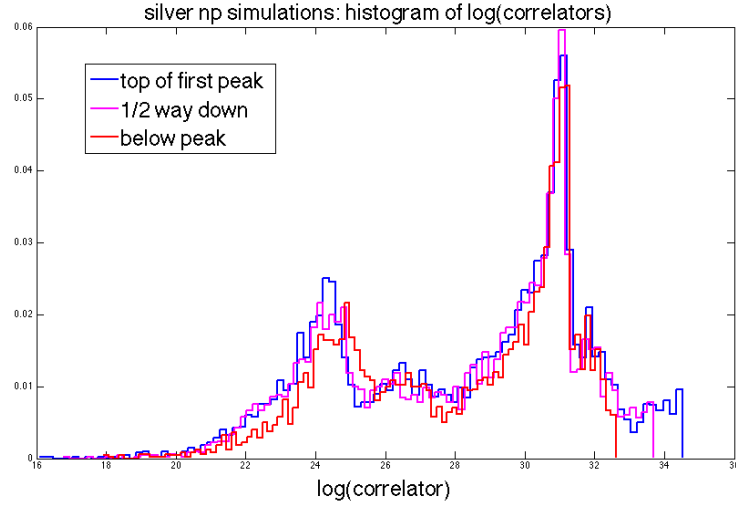

Figure 4: histogram of mean of log(correlators) for NP simulations at 3 ψ values showing exponential variation

Note that TEM evidence suggests that internal twinning of the crystalline order within the NPs is expected [ref], so that the above model may be too simplistic.

6) **materials and methods**

Our samples consisted of silver NPs suspenenin in glycerol solution. Each particle was roughly 20 nanometers in size, but we observed some shots giving signals from particles that were substantially larger. It was important that the particles remained fixed during each exposure, so the sample was cooled to 100 Kelvin using a nitrogen cryo jet. This

4

opposed any heating due to the X-ray beam. The NPs were suspended in a glycerol-based antifreeze in order to prevent the formation of solvent crystals at the low temperature. By monitoring the intensity at constant scattering angle one can check for sample damage and diffusion (Figure needed), both attributes that the CXS signal is extremely sensitive to. To house the solutions we used kapton capillaries with a 500 and 600 micron inner and outer diameter respectively. Kapton scatters into relatively lower angles as does glycerol, hence we did not anticipate corrupting our silver NP signal with a large background.

The experiment was conducted at the micro-crystallography beamline (12-2) at SSRL. Samples were prepared a day early and stored in a liquid nitrogen bath. Samples were loaded and oriented in the X-ray beam using the Stanford Automated Mounting System (SAM) , controllable from the experimental hutch. Using a liquid nitrogen-cooled double crystal monochromator we tuned the beam energy to 17 keV. The beam was focused down to about 15x15 ?m2 using Rh coated Kirkpatrick-Baez mirrors. Images were taken using a Dectris Pilatus 6M pixel detector.

Our goal was to record as many images as possible, each one representing a different ensemble of fixed particle orientations. The sample holder was equipped to automatically rotate the capillary about its longitudinal axis. The capillary was oriented such that its longitudinal axis was perpendicular to the beam (Figure needed) and then it was rotated through a 150 degree angle. The photon counts were read out and reset every 0.7 second and every 0.3 degrees or rotation, giving us 500 shots per 150 degree rotational scan. This was deemed an optimal timing to simultaneously maximize signal and minimize damage and heating. The beam was shining on the capillary for the duration of the scan, hence the center of the capillary was constantly heated. However, this effect was negligible given the path length of the beam through the sample (500 ?m). Between scans we moved the capillary longitudinally, so as to always probe different regions of the sample, and hence different ensembles of particle orientations.

7. references
1. Wochner
2. Kam
3. Kirian et al
4. TEM paper